

Dark Matter and Higgs Bosons in the MSSM

Tao Han^a, Zhen Liu^a, Aravind Natarajan^b

^a*Pittsburgh Particle physics, Astrophysics, and Cosmology Center,
Department of Physics and Astronomy, University of Pittsburgh,
3941 O'Hara St., Pittsburgh, PA 15260, USA*
than@pitt.edu
zhl61@pitt.edu

^b*McWilliams Center for Cosmology, Carnegie Mellon University,
Department of Physics, 5000 Forbes Ave, Pittsburgh PA 15213, USA*
anat@andrew.cmu.edu

ABSTRACT: We investigate dark matter (DM) in the context of the minimal supersymmetric extension of the standard model (MSSM). We scan through the MSSM parameter space and search for solutions that (a) are consistent with the Higgs discovery and other collider searches; (b) satisfy the flavor constraints from B physics; (c) give a DM candidate with the correct thermal relic density; and (d) are allowed by the DM direct detection experiments. For the surviving models with our parameter scan, we find the following features: (1) The DM candidate is largely a Bino-like neutralino with non-zero but less than 20% Wino and Higgsino fractions; (2) Constraints from the Higgs sector and rare b decay measurements exclude the low mass region favored by the DAMA, CoGeNT, and CRESST experiments; (3) The relic density requirement clearly pins down the solutions from the Z and Higgs resonances (Z, h, H, A funnels) and co-annihilations; (4) Future direct search experiments will likely fully cover the Z, h funnel regions, and H, A funnel regions as well except for the “blind spots”; (5) Future indirect search experiments will be more sensitive to the CP-odd Higgs exchange due to its s -wave nature; (6) The branching fraction for the SM-like Higgs decay to DM can be as high as 8%, while those from heavier Higgs decays to neutralinos and charginos can be as high as 20%. We show that collider searches provide valuable information complementary to what may be obtained from direct detections and astroparticle observations, and that the Higgs bosons may play an essential role.

Contents

1. Introduction	1
2. Dark matter relic density	3
3. The MSSM parameters relevant to DM studies	4
4. Current Constraints and the Scanning Results	6
4.1 Constraints from the Higgs searches and the flavor sector	6
4.2 Confronting the direct and indirect searches	7
4.3 Scanning results	8
5. Discussions	13
5.1 The nature of the DM	13
5.2 Lower limit on the spin-independent cross section	15
5.3 Connection to the indirect searches	15
5.4 Implication of LSP for Higgs physics	17
5.5 Consequences of co-annihilation	18
6. Summary and Conclusions	18
A. Relic density calculation	26

1. Introduction

Observations of the cosmic microwave background, gravitational lensing, clustering of galaxies, galactic rotation curves, etc. have provided compelling evidence for the existence of Dark Matter (DM), which is likely to be of particle origin. One of the best motivated candidates for DM is the Weakly Interacting Massive Particle (WIMP), a good example of which is the Lightest Supersymmetric Particle (LSP) (for reviews, see [1–3]). If WIMPs exist in the Galaxy, they may be detected through direct search experiments [4–11]. The DAMA experiment [4] has detected an annual modulation in the measured recoil spectrum at the 8.9σ level, consistent with the presence of WIMP DM in the Galaxy. More recently, the CoGeNT [5] and CRESST [6] experiments have also obtained results that are consistent with low mass WIMP DM. On the other hand, these results have been challenged by other experiments such as XENON-10 [7], XENON-100 [8] and more recently TEXONO [12], which have excluded the parameter space favored by the DAMA, CoGeNT, and CRESST experiments. Complementary to the direct searches, indirect detection experiments include the Fermi gamma ray space telescope [13], Air Cherenkov Telescopes [14–16], and

the Wilkinson Microwave Anisotropy Probe (WMAP) [17, 18]. The WMAP observations place a lower limit on the particle mass $m_\chi \gtrsim 10$ GeV, assuming a velocity-independent annihilation cross section $\langle\sigma_a v\rangle = 1 \text{ pb}\times c$ [19–24]. The non-observation of gamma rays from DM annihilation in the nearby dwarf galaxies [13, 25] has been used to place constraints on the DM particle mass $m_\chi \gtrsim 40$ GeV, for neutralino annihilation to the $b\bar{b}$ channel with a velocity-independent cross section $\langle\sigma_a v\rangle = 1 \text{ pb}\times c$, although these bounds would be relaxed with a more general analysis including the velocity-dependent contributions [26].

On the other hand, the LHC experiments have made a historic discovery of the long-sought-after Higgs boson predicted by the Standard Model (SM). The experiments also show no evidence for Beyond-SM Higgs bosons, nor other new physics such as Supersymmetry (SUSY) etc. with the current data, seemingly in favor of heavy colored sparticles [27–31]. Several authors have recently studied the present LHC data and the implications for DM, as well as the possibility that future LHC data will provide information to the DM puzzle [32–51]. Although the SUSY parameter space has been significantly reduced due to the absence of a SUSY signal at the LHC and due to the constraining properties of the SM-like Higgs boson, a dark matter candidate can still be readily accommodated in SUSY theories.

With the ever increasing experimental sensitivity of DM detection experiments, we are motivated to explore to what extent DM properties have been constrained by the results from particle accelerator experiments. Our goal is to systematically examine the complementarity between DM direct detection experiments, indirect detection searches, and collider experiments, and in particular explore the potential pivotal role played by the Higgs bosons. We perform a comprehensive study in the framework of the minimal supersymmetric extension of the standard model (MSSM). We impose the following constraints on our model considerations:

- (1) **Relic abundance:** The neutralino LSP constitutes all the cold DM, consistent with the cosmological observations [17, 18].
- (2) **Collider constraints:** The MSSM parameter space satisfies all collider constraints from the Higgs boson searches and has a SM-like Higgs boson near 126 GeV.
- (3) **Flavor constraints:** The parameter space satisfies the flavor constraints from $b \rightarrow s\gamma$ [52], and $B_s \rightarrow \mu^+\mu^-$ [53].

We further check the consistency of the annihilation rate at zero velocity $\langle\sigma_a v\rangle(v \rightarrow 0)$ with CMB observations, and the absence of gamma rays from nearby dwarf galaxies [13, 25]. It is known that the spin-independent WIMP-nucleon elastic scattering cross section obtained by the XENON-100 experiment [8] puts a very strong bound on the MSSM parameter space. We find that the surviving region has characteristic features, notably a Bino-like LSP. What is most interesting to us is that all these scenarios would lead to definitive predictions for the LHC experiments, that can be verified by the next generation of direct/indirect search experiments such as LUX [10] and XENON-1T [11].

The rest of the paper is organized as follows. In Section 2, we compute the WIMP relic density in a model-independent manner. We emphasize the importance of including the effect of velocity-dependent annihilation $\langle\sigma_a v\rangle = a + bv^2 + \mathcal{O}(v^4)$, which is crucial

when the b term from the p -wave is not negligible. This will have direct consequences in the interpretation of indirect search results. In Section 3, we discuss our technique for scanning the MSSM parameter space. In Section 4, we present our results, and discuss the experimental constraints from the Higgs and flavor searches. We also discuss the constraints on the parameter space imposed by the XENON-100 search for spin-independent scattering, as well as the Super-K and IceCube/DeepCore limits on spin-dependent scattering. We show that future experiments such as LUX and XENON-1T will likely probe the natural supersymmetric parametric space consistent with the LSP constituting all the DM. We present extensive discussions of our results in Section 5 and finally draw our conclusions in Section 6. Details of the relic density calculation are presented in the Appendix.

2. Dark matter relic density

Within the Standard Cosmology, we evaluate the thermal history of the dark matter [1, 2]. We assume that the WIMP, generically denoted by χ , constitutes all of the thermal DM. Let us define the DM relic density Ω_χ as the ratio of the DM mass density at the present epoch to the critical mass density (ρ_{crit}). The well-measured value from WMAP9, ACT, SPT, SNLS3, BAO, and H0 [18] is obtained

$$\Omega_\chi h^2 = \frac{m_\chi n_\chi}{\rho_{\text{crit}}/h^2} = 0.1148 \pm 0.0019. \quad (2.1)$$

The number density of WIMPs at time t , $n_\chi(t)$, can be obtained by solving the Boltzmann equation (see Appendix for details). The annihilation cross section (σ_a) characterizes the WIMP dynamics for a given theory. Since WIMPs are non-relativistic at freeze-out, the velocity averaged cross section $\langle\sigma_a v\rangle$ may be expanded in v , customarily written as

$$\frac{\sigma_a v}{1 \text{ pb} \times c} = a + bv^2 + \mathcal{O}(v^4), \quad \frac{\langle\sigma_a v\rangle}{1 \text{ pb} \times c} = a + \frac{6b}{x} \quad \text{with } x = \frac{m_\chi}{T}, \quad (2.2)$$

where the traditional units are $1 \text{ pb} \times c = 3 \times 10^{-26} \text{ cm}^3/\text{s}$. Simple threshold arguments indicate that s -wave annihilation contributes dominantly to a , while p -wave annihilation contributes only to b . Requiring that the thermal relic density satisfy the measured value gives us the cross section. This leads to the result:

$$\Omega_\chi h^2 \approx 0.11 \Rightarrow \langle\sigma_a v\rangle \approx 2.18 \times 10^{-26} \text{ cm}^3/\text{s}. \quad (2.3)$$

Fig. 1(a) shows the evolution of the number of relativistic degrees of freedom, from [54]. We show the WIMP number density approaching the present day value in Fig. 1(b) for $m_\chi = 100 \text{ GeV}$ for the extreme cases $b = 0$ and $a = 0$. The range of a and b values versus the WIMP mass is shown in Fig. 1(c). For a WIMP mass above around 4 – 5 GeV, a remains almost constant for arbitrary WIMP masses when b is of negligible value, reflecting the “WIMP miracle” that leads to the correct relic density. Below 4 – 5 GeV, somewhat larger values of a and b would be needed to yield the correct relic density, due to the reduction of g at the quark-hadron transition. We will not explore the very low mass region any further in this work. The interplay between a and b follows a linear relation empirically, and is shown in Fig. 1(d) for various WIMP mass values.

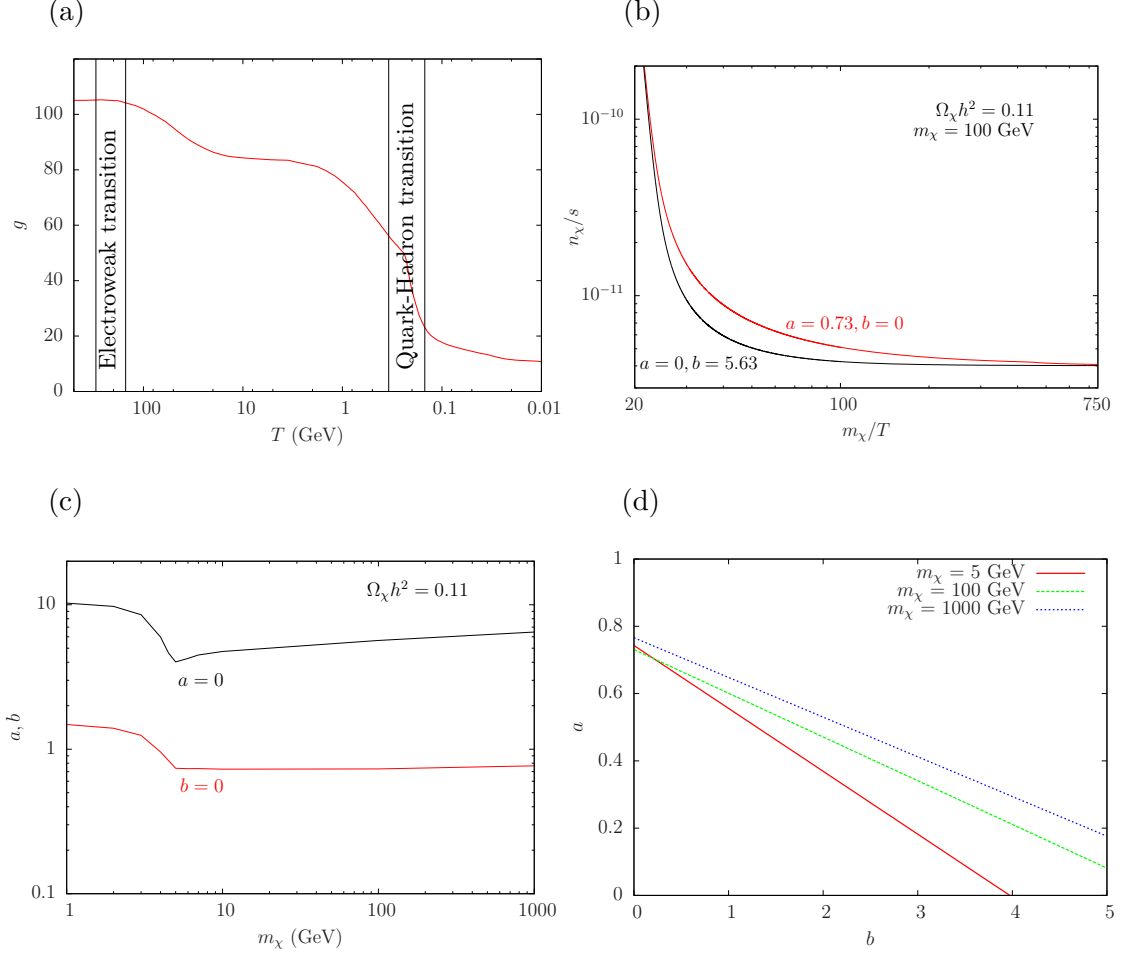


Figure 1: (a) The number of relativistic degrees of freedom as a function of temperature. The relic density $\Omega_\chi h^2 = 0.11$; (b) WIMP number density evolution with temperature for illustrative values of a, b with $m_\chi = 100$ GeV, (c) a, b values versus the WIMP mass, (d) a versus b for $m_\chi = 5, 100$, and 1000 GeV.

3. The MSSM parameters relevant to DM studies

In SUSY theories with conserved R-parity, the lightest supersymmetric particle (LSP) is a viable WIMP DM candidate. For both theoretical and observational considerations [1, 2, 55–57], it is believed that the best candidate is the lightest Majorana mass eigenstate which is an admixture of the Bino (\tilde{B}), Wino (\tilde{W}_3), and Higgsinos ($\tilde{H}_{d,u}$), with the corresponding soft SUSY breaking mass parameters M_1 , M_2 , and the Higgs mixing μ , respectively. The neutralino mass matrix in the Bino-Wino-Higgsino basis is given by

$$M_{\text{neut}} = \begin{bmatrix} M_1 & 0 & -m_Z \cos \beta \sin \theta_w & m_Z \sin \beta \sin \theta_w \\ 0 & M_2 & m_Z \cos \beta \cos \theta_w & -m_Z \sin \beta \cos \theta_w \\ -m_Z \cos \beta \sin \theta_w & m_Z \cos \beta \cos \theta_w & 0 & -\mu \\ m_Z \sin \beta \sin \theta_w & -m_Z \sin \beta \cos \theta_w & -\mu & 0 \end{bmatrix},$$

where m_z is the Z boson mass, θ_w the Weinberg angle, and $\tan\beta = v_u/v_d$ is the ratio of the vacuum expectation values for the two Higgs doublets. The lightest neutralino is a linear combination of the superpartners

$$\chi_1^0 = N_{11}\tilde{B} + N_{12}\tilde{W}_3 + N_{13}\tilde{H}_d + N_{14}\tilde{H}_u, \quad (3.1)$$

where N_{ij} are the elements of the matrix N that diagonalize M_{neut} :

$$N^* M_{\text{neut}} N^{-1} = \text{diag}\{m_{\chi_1^0}, m_{\chi_2^0}, m_{\chi_3^0}, m_{\chi_4^0}\}. \quad (3.2)$$

The eigenvalues of M_{neut} are the masses of the four neutralinos. An interesting limit is $m_z \ll |M_1 \pm \mu|$ and $|M_2 \pm \mu|$, in which case, the mass eigenstates (neutralinos χ_i^0) are nearly pure gauge eigenstates (gauginos and Higgsinos). This also implies that large mixing of gaugino and Higgsino components for the mass eigenstates only takes place when M_1 and/or M_2 are nearly degenerate with μ . We will focus only on the lightest neutralino (henceforth denoted by χ_1^0) with a mass $m_{\chi_1^0}$. In particular, we assume that it constitutes the majority of the DM.

Intimately related to the neutralinos is the Higgs sector. The tree level Higgs masses in the MSSM can be expressed in terms of $\tan\beta$ and the CP-odd mass M_A . Radiative corrections enhance the Higgs mass significantly via the top quark Yukawa coupling, the third generation squark mass parameters M_{Q3} , M_{U3} , and the left-right squark mixing A_t . Flavor physics observations from the b -quark sector often serve as stringent constraints and we therefore include the sbottom sector parameters M_{D3} and the squark mixing A_b . The last potentially relevant sector is the stau, which could be light and contribute to the t -channel exchange, co-annihilations to control the relic density. We therefore generously vary the MSSM parameters in the ranges

$$\begin{aligned} 5 \text{ GeV} < |M_1| < 2000 \text{ GeV}, \quad 100 \text{ GeV} < |M_2, \mu| < 2000 \text{ GeV}, \\ 3 < \tan\beta < 55, \quad 80 \text{ GeV} < M_A < 1000 \text{ GeV}, \\ -4000 \text{ GeV} < A_t < 4000 \text{ GeV}, \quad 100 \text{ GeV} < M_{Q3}, M_{U3} < 3000 \text{ GeV}, \\ -4000 \text{ GeV} < A_b < 4000 \text{ GeV}, \quad 100 \text{ GeV} < M_{D3} < 3000 \text{ GeV}, \\ -4000 \text{ GeV} < A_\tau < 4000 \text{ GeV}, \quad 100 \text{ GeV} < M_{L3}, M_{E3} < 3000 \text{ GeV}. \end{aligned} \quad (3.3)$$

The lowest values of M_1 , M_2 and μ control the LSP mass for the WIMP DM. The lower values of 100 GeV for M_2 , μ are dictated by the LEP-2 bound from the largely model-independent chargino searches. The lower limit of $\tan\beta$ is close to the LEP-2 Higgs search exclusion. The lower limit of M_A is chosen to cover the non-decoupling Higgs sector as well as above the LEP-2 bound on the charged Higgs. The upper limit of M_1 , M_2 , μ and the soft SUSY breaking masses in the stop and stau sectors are set with consideration of naturalness [36, 58–62]. The other soft supersymmetry breaking parameters are less relevant for our DM considerations and we therefore set the other trilinear mass parameters to be zero, and the other soft SUSY breaking masses at 3 TeV.

While the natural value of μ is supposed to be close to the electroweak scale, we vary μ up to 2 TeV to capture some interesting futures such as the scenario of “well-tempered

neutralino” [63]. Letting $\mu \approx 2$ TeV would already allow for a severe fine tuning at the level of about 0.04% [58]. Although not our focus, we have included the arbitrary signs for the M_1, M_2, μ parameters. This allows us to see the possible solutions with very specifically chosen parameter relations such as the “blind spots” scenarios [48, 64].

We choose a flat prior for the scanning with a total number of scanned points around 10 million. Several different layers of scanning are performed to account for different experimental constraints, as seen by the corresponding color codes in our plots.

4. Current Constraints and the Scanning Results

The hints of DM detection from the DAMA, CoGeNT, and CRESST experiments have drawn significant interest in considering valid theoretical interpretations. The sensitivity of the DM direct searches have been steadily improving at an impressive pace, notably with the XENON collaboration [7, 8]. The indirect searches from WMAP, Fermi-LAT, and IceCube have also played crucial roles in exploring the nature of the DM particle.

Although the null results of searching for Supersymmetry at colliders have significantly tightened the viable SUSY parameter region, the bounds on WIMP DM properties are only limited within specific models, most notably in mSUGRA or CMSSM [32, 33]. The direct exploration of the electroweak gaugino sector at the LHC would be very challenging given the hostile background environment and the current search results depend on several assumptions [65, 66]. On the other hand, if we demand the correct WIMP LSP relic abundance from the current observations as in Eq. (2.1), the SUSY parameter space of Eq. (3.3) will be notably constrained in the Higgs and gaugino sectors. We assume a 10% theoretical uncertainty in the calculation of the DM relic density [35, 67]. Applying the combined WMAP9 + ACT + SPT + SNLS3 + BAO + H0 result in Eq. (2.1) combined with 10% theoretical uncertainty, we demand that the relic density in our model points be within the following 2σ window

$$0.0915 < \Omega_{\chi_1} h^2 < 0.1381 \quad (4.1)$$

We use the publicly available FEYNHIGGS code [68] as the spectrum calculator. The Higgs constraints are imposed using the HIGGSBOUNDS package [69] with our additional modifications. We modify the codes to include the most recent LHC constraints.¹ The standard SLHA [70] output recorded is then supplied to the MICROMEGAS code [71] which computes the DM relic density, direct/indirect search cross sections and flavor calculations. This is done to avoid any possible inconsistency due to the subtle differences in the spectrum calculator, particularly the lack of accuracy in the default approximate diagonalization routine for the neutralino mass matrix.

4.1 Constraints from the Higgs searches and the flavor sector

The discovery of a SM-like Higgs boson h as well as the upper limits on difference channels for the other Higgs bosons A, H, H^\pm shed much light on the electroweak sector, and can

¹We have implemented the latest LHC search results from ATLAS (<http://atlas.ch>) and CMS (<http://cms.web.cern.ch>).

thus guide us for DM studies. When scanning over the SUSY parameter space as in Eq. (3.3), and requiring the correct WIMP LSP relic abundance to be within the 2σ window in Eq. (4.1), we further require the theory to have a SM-like Higgs boson, and to accommodate all the current constraints from the Higgs searches:

$$\begin{aligned}
& 123 \text{ GeV} < m_h < 128 \text{ GeV}, \quad \sigma_{\gamma\gamma} > 0.8 \sigma_{\gamma\gamma}(SM), \\
& \text{plus Higgs search bounds from LEP, Tevatron, LHC,} \\
& \text{plus LEP bounds on the chargino mass } (\geq 100 \text{ GeV}) \\
& \text{and the slepton mass } (\geq 80 \text{ GeV}).
\end{aligned} \tag{4.2}$$

Due to the correlation of the Higgs couplings, the requirement of the $\sigma_{\gamma\gamma}$ cross section effectively sets the SM-like values for σ_{WW} , σ_{ZZ} as well.

The absence of tree-level flavor changing neutral currents (FCNC) in the SM puts strong constraints on new physics. We consider two processes that have been observed to be consistent with the SM prediction and thus provide constraints on the MSSM parameter space. The first process is $b \rightarrow s\gamma$ [72], for which the branching fraction is sensitive to the charged Higgs boson and supersymmetric particles (e.g. chargino/stop) in the loop. The world average of the branching fraction of this channel [73] is $(3.55 \pm 0.24 \pm 0.09) \times 10^{-4}$ in good agreement with the standard model prediction [74–76] $(3.15 \pm 0.23) \times 10^{-4}$.

The second process is $B_s \rightarrow \mu^+\mu^-$, which receives a large contribution in the MSSM proportional to $(\tan^6 \beta / m_A^4)$ [77]. The LHCb collaboration has recently announced the first discovery [53] of this very rare decay and the branching ratio for this process was found to be $(3.2^{+1.4}_{-1.2} {}^{+0.5}_{-0.3}) \times 10^{-9}$ in good agreement with the standard model prediction of $(3.23 \pm 0.27) \times 10^{-9}$ [78]. They also announced a 95% confidence level upper bound of 5.1×10^{-9} on $\text{BR}(B_s \rightarrow \mu^+\mu^-)$. We adopt this more stringent value to put constraints on $\text{BR}(B_s \rightarrow \mu^+\mu^-)$.

We adopt the theoretical uncertainties from the SM predictions. We note that the uncertainties from experiments are of the same order of magnitude as the theoretical uncertainty for $\text{BR}(b \rightarrow s\gamma)$, and thus the latter become very important. In light of these precision results, we require our MSSM solutions to be within 2σ of the observed value:

$$\begin{aligned}
2.86 \times 10^{-4} < \text{BR}(b \rightarrow s\gamma) &< 4.24 \times 10^{-4}, \\
\text{BR}(B_s \rightarrow \mu^+\mu^-) &< 5.1 \times 10^{-9}.
\end{aligned} \tag{4.3}$$

4.2 Confronting the direct and indirect searches

Thus far, the most stringent constraints on the spin-independent elastic scattering cross section (σ_p^{SI}) come from the XENON-100 experiment. The results from the XENON experiment challenge the signal hints from DAMA, CoGeNT and CRESST in the low mass region of $m_\chi \approx 10 \text{ GeV}$, and cut deeply into the parameter space with $\sigma_p^{\text{SI}} \sim 2 \times 10^{-9} \text{ pb}$ at $m_\chi \sim 60 \text{ GeV}$. Limits on the spin-dependent cross section are not as constraining. We account for the bounds from the Super-Kamiokande [79], and the IceCube/DeepCore [80]

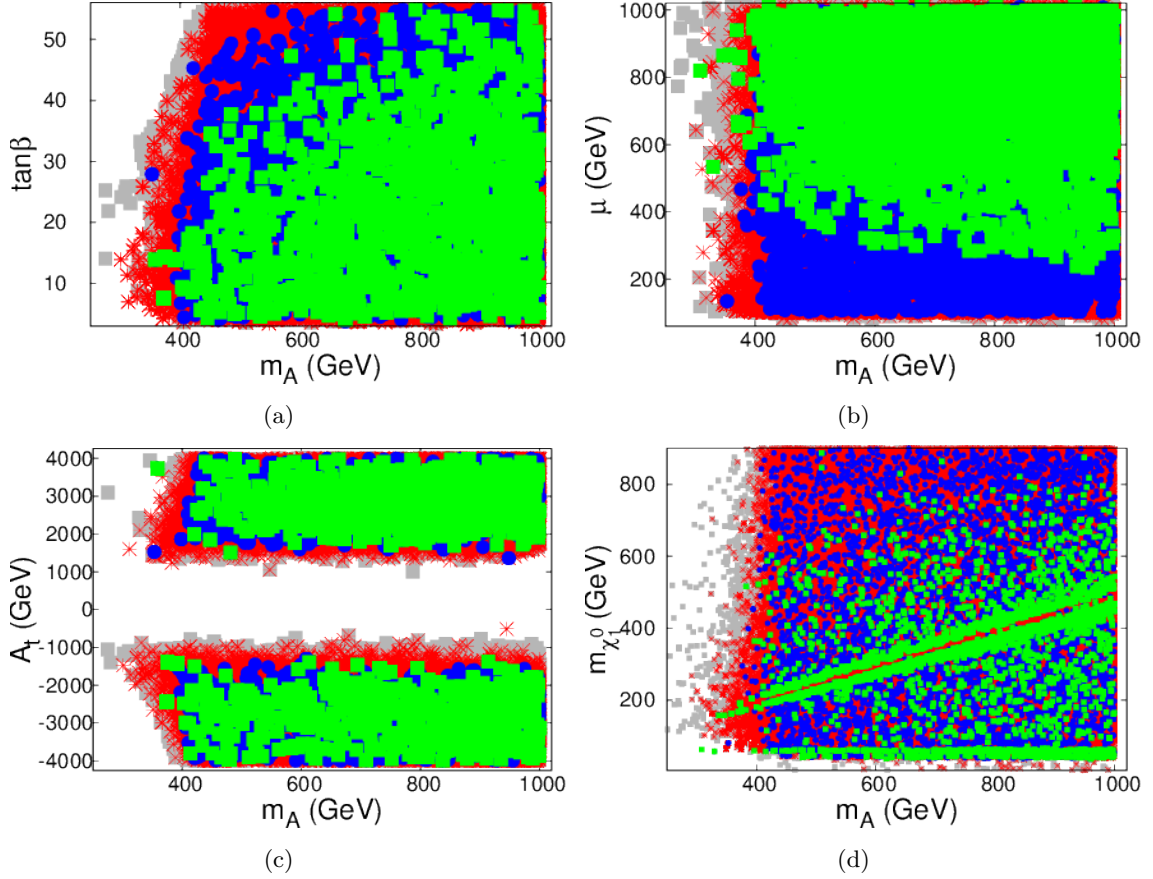


Figure 2: Allowed parameter regions versus the CP-odd Higgs boson mass m_A , for (a) $\tan\beta$, (b) the Higgs mixing parameter μ , (c) stop mixing parameter A_t and (d) LSP DM mass m_{χ} , respectively. All points pass the collider and Higgs constraints of Eq. (4.2). The grey squares require that the DM does not overclose the Universe; the red stars in addition satisfy the flavor constraints of Eq. (4.3); the blue disks are consistent with the LSP being all of the DM (i.e. predicts the correct relic density of Eq. (4.1)). The green squares pass the XENON-100 direct search bound in addition to the other requirements.

experiments that are sensitive to the spin-dependent scattering of DM with Hydrogen in the sun. We also take into account bounds obtained by the Fermi satellite from the absence of gamma rays from the nearby dwarf galaxies.

4.3 Scanning results

We now present our results for the allowed parameter regions in Figs. 2–9. In Fig. 2, we show the parameter points passing the Higgs constraints in Eq. (4.2) versus the CP-odd Higgs boson mass m_A , for (a) $\tan\beta$, (b) Higgs mixing parameter μ , (c) stop mixing parameter A_t and (d) DM mass m_{χ} , respectively. These allowed parameter regions are shown in Fig. 3 for branching fractions (a) $\text{BR}(b \rightarrow s\gamma)$ and (b) $\text{BR}(B_s \rightarrow \mu^+\mu^-)$ versus $\tan\beta$. We show from the same set of points, the Wino mass parameter M_2 and the Higgsino mass parameter μ versus the Bino mass parameter M_1 in Figs. 4(a) and (b). We show the

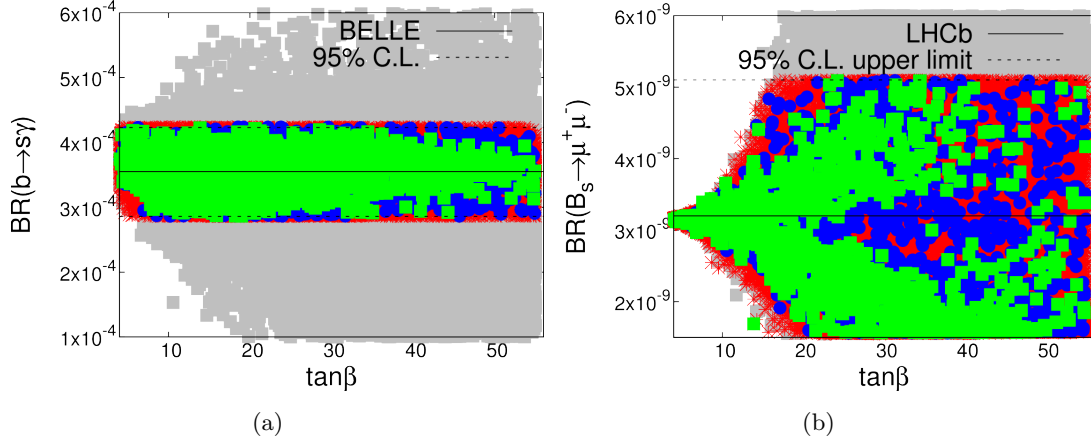


Figure 3: Allowed branching fraction regions versus $\tan\beta$, for (a) $b \rightarrow s\gamma$, (b) $B_s \rightarrow \mu^+\mu^-$. The corresponding experimental central values and 2σ bands are plotted on each panel. Symbols and legends are the same as in Fig. 2.

second and third neutralino masses $m_{\chi_2^0}, m_{\chi_3^0}$, the light stau mass and the light stop mass versus the LSP mass m_χ in Figs. 4(c), (d), (e) and (f). In the above Figures 2–4, all points satisfy the collider, and Higgs search requirements in Eq. 4.2. The grey squares show MSSM models that do not overclose the universe. The red stars in addition satisfy the flavor requirements in Eq. (4.3). The blue disks represent the models that give the correct relic density in Eq. (4.1). Finally, the green squares pass the severe XENON-100 direct search bound on the WIMP-proton spin-independent elastic scattering.

The results obtained here are consistent with the existing literature on the studies at the LHC [81,82]. We make the following important observations:

(1). Higgs constraints (grey squares): We start with points that do not overclose the universe and satisfy the collider search requirements in Eq. (4.2). We reproduced the known results that there are two surviving regions:

(i) The non-decoupling regime where $m_A \sim 95 - 130$ GeV, the heavy CP-even Higgs (H) is SM-like, and the light CP-even Higgs (h) is nearly degenerate in mass with the CP-odd Higgs (A). This region is particularly interesting since it leads to rich collider phenomenology and favors a light WIMP mass $m_\chi \lesssim 50$ GeV. These points are not shown on the plots since they are disfavored by the flavor constraints, as discussed next.

(ii) The decoupling regime where $m_A \gtrsim 250$ GeV, the light CP-even Higgs is SM-like, and the heavy CP-even Higgs is nearly degenerate in mass with the CP-odd Higgs. This regime is difficult to observe at the LHC when $m_A \gtrsim 400$ GeV and $\tan\beta \sim 10 - 20$ in traditional SM Higgs search channels due to severely suppressed couplings to the gauge bosons.

(2). Flavor constraints (red stars): The two decay processes $b \rightarrow s\gamma$ and $B_s \rightarrow \mu^+\mu^-$ are the most constraining ones. The experimental central values are plotted on the calculated

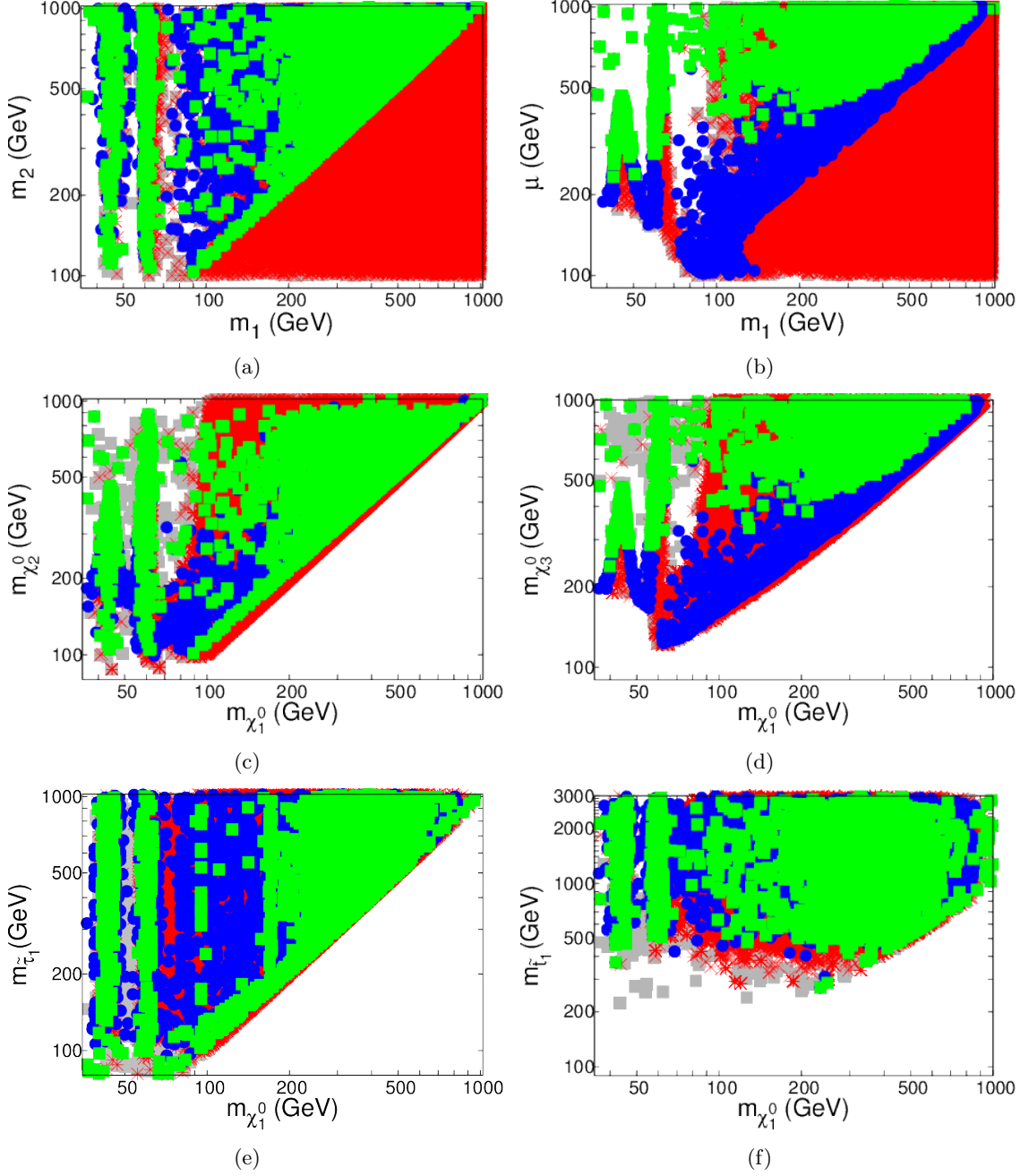


Figure 4: Allowed parameter regions for (a) μ and (b) M_2 versus the Bino mass parameter M_1 . (c) and (d) show the second and the third neutralino masses $m_{\chi_2^0}$, $m_{\chi_3^0}$ for different values of the DM mass. (e) and (f) show the stau mass $m_{\tilde{\tau}}$ and stop mass $m_{\tilde{t}}$ respectively, versus the DM mass m_{χ} . Symbols and legends are the same as in Fig. 2.

branching fractions in Fig. 3 on each panel, along with 2σ bands, which is summarized in Eq. (4.3). These flavor constraints prefer lower $\tan\beta$ values and essentially remove the light Higgs (H^0, A^0, H^\pm) solutions in the non-decoupling region in our generic scan. The

solutions with a light LSP of $m_\chi \lesssim 30$ GeV are also eliminated. Our results are in good agreement with the existing studies [38, 47]. Further improvements in the $B_s \rightarrow \mu^+ \mu^-$ measurement would strongly constrain the large $\tan\beta$ and low m_A region. However, we have not tried to exhaust parameter choices with possible cancelations among different SUSY contributions, and some sophisticated scanning may still find solutions with certain degrees of fine-tuning [83].

(3). Relic density requirement (blue disks): Merely requiring that the LSP does not over-close the universe does not constrain the MSSM parameter space very much, as most clearly seen from the gray squares and red stars in Fig. 4. This is because the Higgsino-like or Wino-like LSPs and NLSPs can annihilate efficiently through gauge bosons and Higgs bosons. Requiring the correct dark matter relic density at the present epoch does constrain the parameter space significantly. We see the preference for $\mu > M_1$ and $M_2 > M_1$, as in Figs. 4(a) and (b). Otherwise the Higgsino or Wino LSP would annihilate too efficiently, and result in too little dark matter. Nevertheless, we do find a nearly degenerate region of a Bino LSP and Wino NLSPs as seen in Fig. 4(c), which is best characterized by the “well-tempered” scenario [63]. This scenario, however, seems to be less implementable with Higgsino NLSPs as seen in Figs. 4(b) and (d), if μ is not much greater 1 TeV. Importantly for our interests, we see prominent strips near $m_\chi \sim m_Z/2$, $m_h/2$ which are the Z and Higgs funnel regions. Interestingly, as seen in Fig. 2(d), there is a region of depletion near $m_A \approx 2m_\chi$, indicating the very (too) efficient annihilation near the A^0 funnel in the s -channel that is removed by the correct relic density requirement. This is a result of a lower bound on the LSP-Higgsino component N_{13} that we will discuss later.

(4). Direct search bounds (green, yellow and magenta squares): The results from DM direct searches can be translated to spin-independent cross sections and thus to the MSSM parameters. This is shown in Fig. 5, where all the points in the colored shaded region give the correct relic abundance in Eq. (4.1), satisfy the collider constraints in Eq. (4.2) and the flavor constraints in Eq. (4.3). The parameter space favored by the DAMA, CoGeNT and CRESST experiments, as well as the stringent bound from the XENON-100 experiment are plotted. We see that there are no surviving points in the low mass region and the blue region is further excluded by the XENON-100 experiment². As seen in Fig. 2(a), lower $\tan\beta$ and higher m_A values are preferred. Figures 2(b) and 4(b) show the lower bound $\mu > 200$ GeV. This consequently leads to a heavier χ_3^0 as seen in 4(d), while χ_2^0 could be still as light as the LSP χ_1^0 as seen in 4(c).

The most important observation from our study is that the surviving points are quite characteristic. We can identify the following classes of predictive features for the LSP DM from Fig. 5.

- I-A (green) $\chi_1^0 \chi_1^0 \rightarrow Z \rightarrow SM$ predicts $m_\chi \approx m_Z/2 \sim 45$ GeV, the Z -funnel.
- I-B (green) $\chi_1^0 \chi_1^0 \rightarrow h \rightarrow SM$ predicts $m_\chi \approx m_h/2 \sim 63$ GeV, the h -funnel.

²It should be noted that the theoretical calculation of the spin-independent cross section may have significant uncertainties [84, 85].

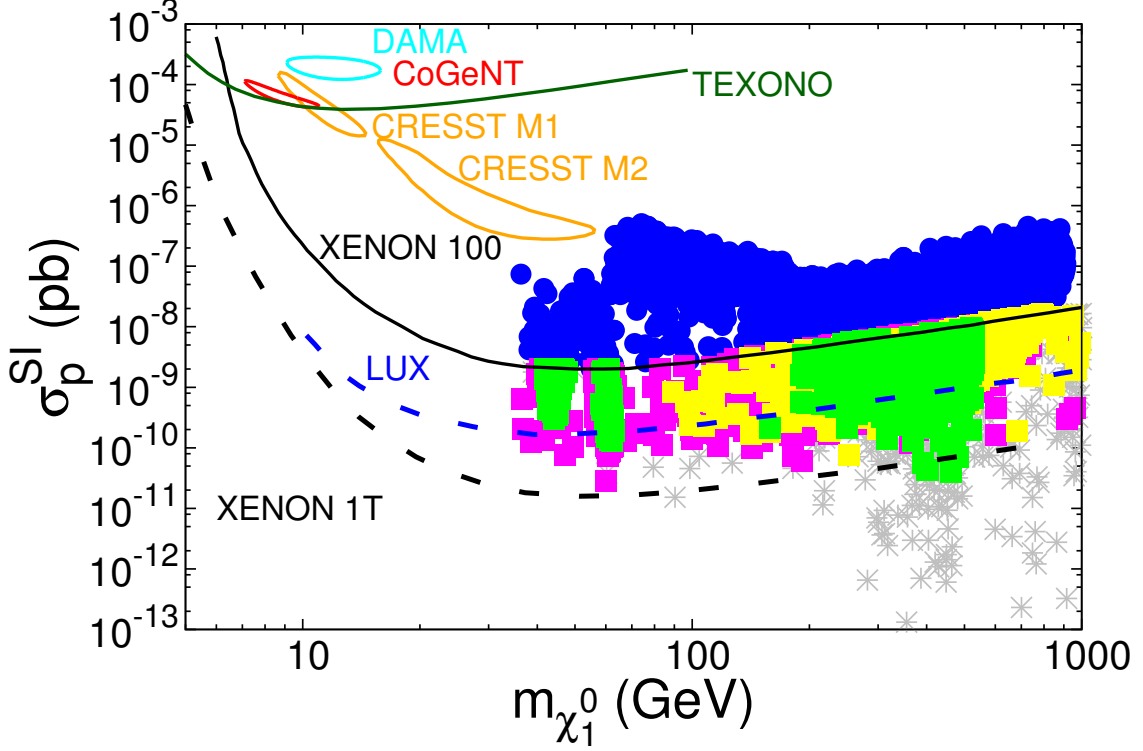


Figure 5: Spin-independent cross section versus the DM mass $m_{\chi_1^0}$. All the points in the colored shaded region give the correct relic abundance in Eq. (4.1), satisfy the collider constraints in Eq. (4.2) and the flavor constraints in Eq. (4.3). The green region represents the model points with the Z and Higgs resonances. The Z funnel and h funnel regions are clearly visible for WIMP masses around half the Z mass and half the Higgs mass. The yellow points represent the region of co-annihilation with Wino-like/Higgsino-like NLSPs. The magenta points represent the region with $\tilde{\tau}$, $\tilde{\nu}_\tau$, \tilde{b} , \tilde{t} contributions. The gray points represent the scenarios with special cancellations when M_1 and μ take opposite signs. The DAMA and CoGeNT contours (3σ) are shown for astrophysical parameters $v_0 = 220$ km/s, $v_{\text{esc}} = 600$ km/s, and for a local density $\rho_0 = 0.3$ GeV/cm³. CRESST contours are 2σ regions, from [6]. The blue region is excluded by the XENON-100 experiment (90% exclusion curve from [8], for $v_0 = 220$ km/s, $v_{\text{esc}} = 544$ km/s, $\rho_0 = 0.3$ GeV/cm³). Recent results from the TEXONO [12] collaboration are shown. Expected exclusion bounds from the ongoing LUX experiment [10] and the future XENON-1T experiment [11] are also shown.

I-C (green) $\chi_1^0 \chi_1^0 \rightarrow H, A \rightarrow SM$ predicts $m_\chi \approx m_{A,H}/2 \sim 0.2-0.5$ TeV, the H/A -funnel.

II-A (yellow) Neutralino/chargino coannihilation [86,87]: $\chi_i^0 \chi_j^0, \chi_i^0 \chi_j^\pm \rightarrow SM$.

II-B (magenta) Sfermion assistance [88-90]: $\chi_1^0 \tilde{\tau}, \chi_1^0 \tilde{t}, \chi_1^0 \tilde{b} \rightarrow SM$; t -channel $\tilde{\tau}, \tilde{\nu}$ in $\chi_i^0 \chi_j^0$.

We categorize model points as scenario I if the difference between the mediator mass and twice the LSP mass is within 8% of the mediator mass, namely

$$|m_{Z,h,A} - 2m_{\chi_1^0}| \leq 0.08 m_{Z,h,A}. \quad (4.4)$$

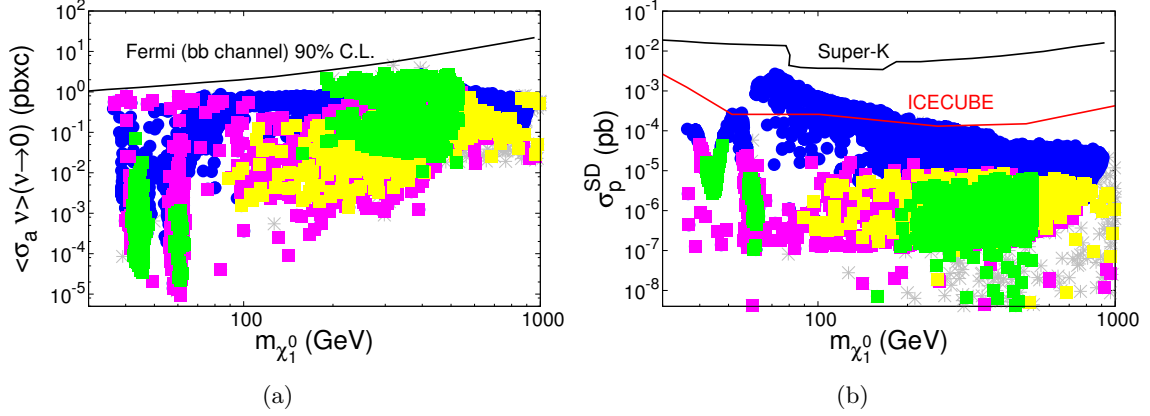


Figure 6: (a) The annihilation cross section $\langle\sigma_a v\rangle$ in the limit $v \rightarrow 0$ along with the 95% exclusion obtained by the Fermi satellite from the absence of gamma rays from the nearby dwarf galaxies [13]. (b) The spin-dependent scattering cross section with a proton, along with the 90% exclusion curves from the Super-K [79] and IceCube [80] experiments. Legends are the same as in Fig. 5.

We categorize model points as scenario II-A if the difference between the LSP mass and neutralino NLSP³ mass is less than 15% of the LSP mass, namely $m_{\chi_2^0} - m_{\chi_1^0} < 0.15m_{\chi_1^0}$. Other cases are categorized as scenario II-B. Our classification and categorization have been verified by investigating a fraction of our generated model points and looking into their individual contributing annihilation channels.

(5). Indirect search bounds:

There exist cosmological bounds from the indirect search for DM signals. We present the annihilation cross section $\langle\sigma_a v\rangle$ in the limit $v \rightarrow 0$ (i.e. the v -independent component) versus the LSP DM mass in Fig. 6(a), along with the 95% exclusion obtained by the Fermi-LAT satellite from the absence of gamma rays from the nearby dwarf galaxies [13]. We see that further improvement from the measurement at the Fermi-LAT will reach the current sensitivity range. The spin-dependent scattering cross section with a proton is shown in Fig. 6(b), along with the 90% exclusion curves from the Super-Kamiokande experiment [79] and the IceCube constraint from DM annihilation in the Sun [80]. We see that IceCube results are cutting into the relevant parameter region closing the gap from the direct searches, although the bounds from the indirect searches are not quite as strong as that from XENON-100.

5. Discussions

5.1 The nature of the DM

Experimental results from the collider searches, the b -quark rare decays and the direct DM searches, combined with the relic density requirement have put very stringent constraints

³This is almost always true because we have a very Bino-like LSP. For cases with $\tilde{\tau}_1$, \tilde{t}_1 NLSP with the sfermion coannihilation mechanism, they fall into scenario II-B automatically.

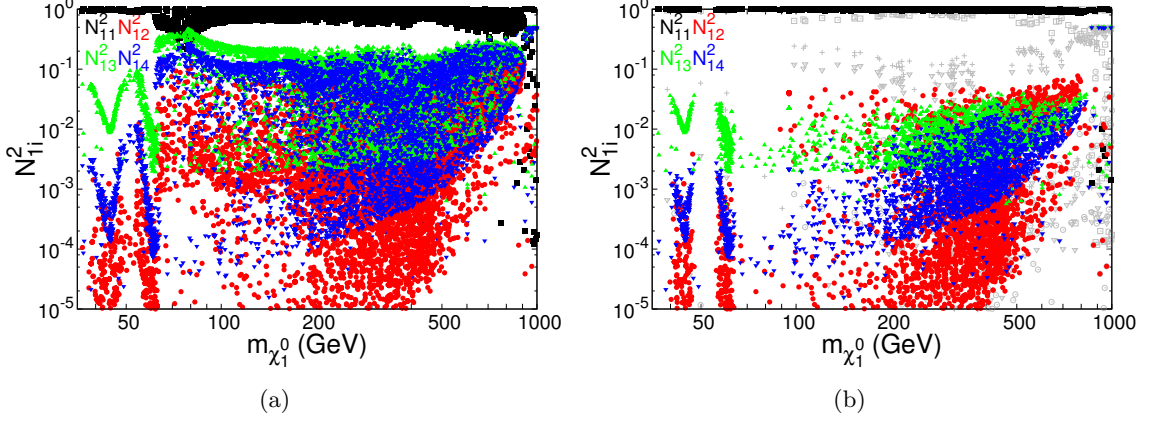


Figure 7: The gaugino and Higgsino fractions of the LSP versus $m_{\chi_1^0}$ (a) consistent with the relic density, collider, and flavor constraints, (b) consistent with XENON-100 in addition to the other requirements. The gray points represent the results for M_1 and μ to have opposite signs and the corresponding fractions N_{11}^2 , N_{12}^2 , N_{13}^2 and N_{14}^2 are denoted by hollow squares, circles, daggers and hollow triangles, respectively.

on the SUSY parameter space. This in turn could have significant implications for searches at future collider experiments. Of primary importance is the nature of the LSP. We show the gaugino and Higgsino fraction (N_{1i}^2) of the neutralino LSP versus its mass in Fig. 7, consistent with all collider and flavor measurements as well as the correct relic density. From Fig. 7(a), we note that the surviving points are mostly Bino-like (N_{11}^2 , as shown by the black dots), with lower fractions for Wino-like (N_{12}^2 , red dots) and Higgsino-like (N_{13}^2 , N_{14}^2 , green and blue dots, respectively). As noted earlier, this is because Wino-like and Higgsino-like LSP’s annihilate very efficiently via SU(2) gauge interactions resulting in too little dark matter at the present epoch. Yet, the LSP could not be purely Bino-like since it would overclose the Universe. In the region $m_{\chi_1^0} \sim 40$ GeV–60 GeV, the line structures corresponding to the Higgsino components are easily identifiable with the Z and h exchanges.

The XENON-100 direct search plays a crucial role in fixing the DM properties. The surviving points are shown in Fig. 7(b). We see that the Wino and Higgsino fractions of the LSP are further constrained to a smaller fraction. The \tilde{H}_d component comes in with the opposite signs with respect to the \tilde{H}_u and \tilde{W} components. Bino-like LSP becomes more pronounced and the Wino and Higgsino components consist of less than 7% each, rendering the “well-tempered” scenario [63] difficult to realize with large Bino-Wino or Bino-Higgsino mixing. The comparison between Fig. 7(a) and (b) clearly shows the XENON-100 exclusion probes deeply into the Higgsino and Wino components. On the other hand, the \tilde{H}_d component N_{13}^2 must be non-zero, and so is N_{14}^2 for \tilde{H}_u . The non-zero lower bound would have significant implications for direct searches as we will discuss next, although the precise values may depend on the choice of the ranges for M_1 , M_2 and μ .

It is important to note that a relative opposite sign between M_1 and μ could result in a subtle cancellation for the $h\chi\chi$ coupling [48, 64], and thus enlarge the allowed mixing parameters, reaching about 20% Wino/Higgsino mixtures, as shown by the grey points in

Fig. 7(b). This can happen only for a higher LSP mass when co-annihilations or H, A funnels could be in effect.

5.2 Lower limit on the spin-independent cross section

With our assumptions in the MSSM framework and the well-constrained properties of the LSP, we would expect that the DM scattering cross section may be predicted.

It is interesting to ask whether one may derive a lower limit for the spin-independent scattering cross section. This is quite achievable for the Higgs resonance situation. Much effort has been made to derive the neutralino recoil cross sections with nuclei in various SUSY models [56, 91–96]. This cross section mainly receives contributions from h, H exchanges and squark exchanges. Given the current experimental bounds on the masses of the squarks from the LHC [97, 98], the Higgs exchanges dominate. As a good approximation in the decoupling limit $\cos(\alpha - \beta) \simeq 0$, $\tan\beta \geq 3$ and a Bino-like LSP, the neutralino-nucleon cross sections via the Higgs exchanges are of the form [95]:

$$\sigma_{\chi N} \propto \begin{cases} \frac{|N_{11}|^2 |N_{13}|^2}{m_H^4 \cos^2 \beta} (f_{T_s} + \frac{2}{27} f_{TG})^2, & H \text{ exchange,} \\ \frac{|N_{11}|^2 |N_{14}|^2}{m_h^4} (f_{T_u} + \frac{4}{27} f_{TG})^2, & h \text{ exchange.} \end{cases} \quad (5.1)$$

f_{T_s} , f_{T_u} and f_{TG} are parameters measured from nuclear physics experiments. The H exchange benefits from an enhancement factor $(N_{13}/\cos\beta)^2$. When the H is heavy, the h exchange proportional to N_{14}^2 becomes important. Due to our natural choices of parameters as in Eq. (3.3), there exist lower bounds on N_{13}^2 and N_{14}^2 , as shown in Fig. 7, although unnaturally large values of μ and m_A could relax these bounds. Consequently, the LSP spin-independent cross sections at the Z, h funnels, which are mainly from the LSP scattering of a t -channel H exchange, reaches a lower bound, roughly

$$\sigma_p^{SI}(h, H) \gtrsim 10^{-10} \text{ pb.} \quad (5.2)$$

As seen in Fig. 5, this range (green dots) will be probed by the ongoing LUX experiment and will be fully covered by the proposed XENON-1T experiment. Similar argument could be also applicable to the H, A funnel regions, where t -channel h exchange could become dominant. However, an exception is that a subtle cancellation takes place when M_1 and μ take opposite signs [48, 64]. As seen from the grey points in Fig. 5(b), this can happen only for a higher LSP mass when co-annihilations or H, A funnels could be in effect.

In Ref. [99], a parameter-independent lower bounds $\sigma_p^{SI} \gtrsim 2 \times 10^{-12} \text{ pb}$ could be obtained in the mass range $440 \text{ GeV} \lesssim m_\chi \lesssim 1020 \text{ GeV}$ and $\mu > 0$. In the most general pMSSM [46] with much larger M_2, μ parameters, the spin-independent cross section could go lower, depending on the mixing parameters.

5.3 Connection to the indirect searches

The WIMP DM at the present epoch is non-relativistic and we can thus relate the current indirect search via LSP annihilation to that at freeze out [100]. The partial wave properties of the LSP annihilation allow us to understand the various contributions. Fig. 8(a) shows

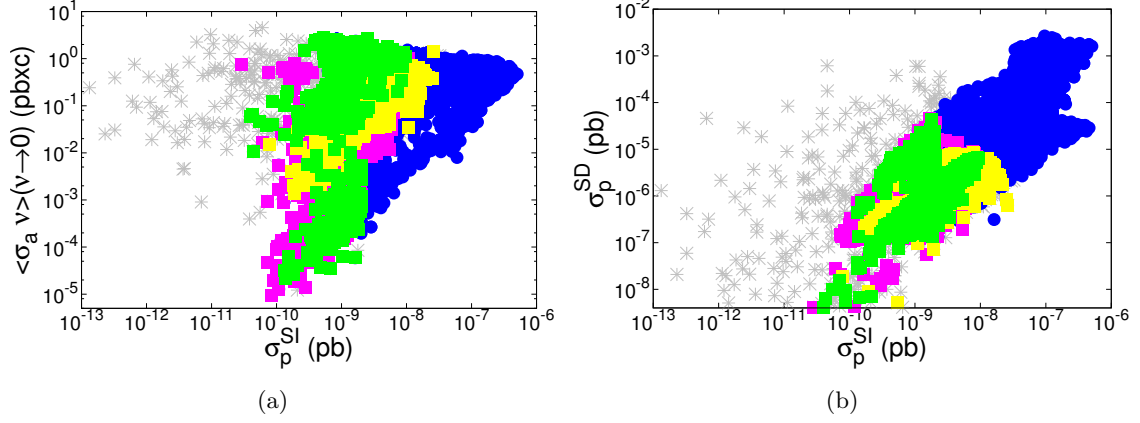


Figure 8: (a) the annihilation cross section $\langle\sigma_a v\rangle(v \rightarrow 0)$ versus the spin independent cross section σ_p^{SI} . (b) the spin-dependent cross section σ_p^{SD} versus the spin independent cross section σ_p^{SI} . Legends are the same as in Fig. 5.

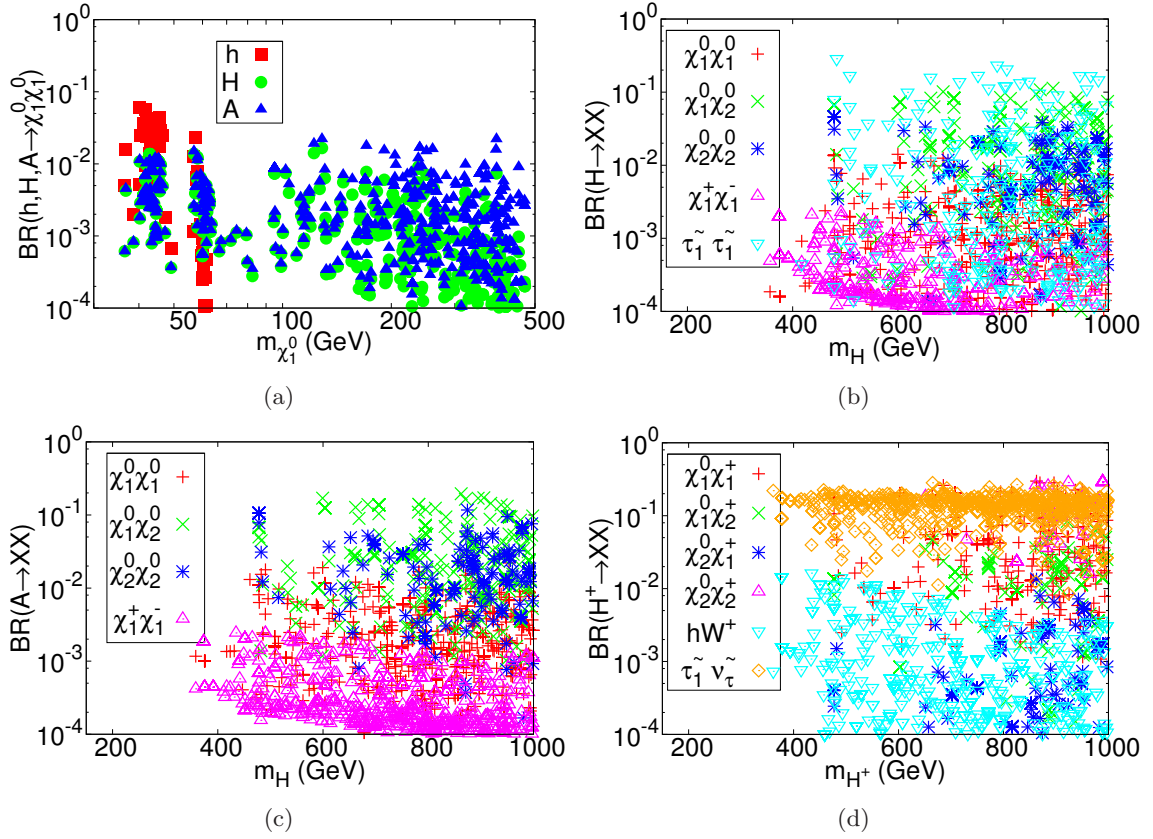


Figure 9: Branching fractions to neutralinos and charginos (a) for h, H, A decays to LSP pair versus the LSP mass, (b) for H , (c) for A , and (d) for H^\pm versus its mass respectively.

the annihilation cross section $\langle\sigma_a v\rangle(v \rightarrow 0)$ versus the spin-independent cross section when scattering off a proton σ_p^{SI} . The model points in green squares near half the Z boson

and near half the 126 GeV Higgs boson in Fig. 6(a) correspond to the low branch of the green squares in Fig. 8(a), due to the p -wave suppression. On the other hand, the s -channel annihilation through A in the mass window 200 GeV \sim 500 GeV in Fig. 6(a) is through s -wave, and thus has a relatively high cross section (indicated by the high branch of green squares). Although the LSP couplings to H and A both are mainly through their Higgsino components N_{14} , the H exchange is via p -wave and thus yields a lower cross section as shown by the middle branch in Fig. 8(a). Finally, we note that the LSP-NLSP co-annihilation (yellow squares) could yield higher cross sections for both direct, and indirect searches, depending on their Wino and Higgsino components. Fig. 8(b) shows the spin-dependent cross section versus the spin-independent cross section, for our different models. Some of the models represented by blue points have a large enough cross section to be probed by IceCube/DeepCore [80]. However, a large spin-dependent cross section implies a proportionally large spin-independent cross section. Thus, all models in blue are excluded by the XENON-100 experiment. Fig. 8 illustrates the connection between spin-dependent and spin-independent measurements, as well as the connection between direct searches and indirect searches. Further improvement of the indirect search sensitivity will soon reach the relevant parameter region, and will probe the A exchange contribution due to its s -wave dominance.

5.4 Implication of LSP for Higgs physics

As shown in Fig. 10, a class of solutions exist with the LSP mass nearly half the mediator Z , h , H , A mass that undergoes a resonant enhancement in annihilation, in the Higgs funnel region. One may expect to see the mediator's invisible decay mode to LSP pairs in collider experiments. Unfortunately, these channels are kinematically suppressed near threshold by the non-relativistic velocity factor. Near the Z peak for example, the search for $Z \rightarrow \chi_1^0 \chi_1^0$ would prove impossible since the branching fraction would be smaller than 10^{-5} due to this suppression. On the other hand, invisible decay channels could be sizable for heavier parent particles. Shown in Fig. 9(a) are the branching fractions of h , H , A to a pair of LSP $\chi_1^0 \chi_1^0$ versus its mass, which would be the invisible mode in collider experiments. It is informative to note that the SM-like Higgs boson receives two distinctive contributions denoted by the red squares

$$\text{BR}_{\text{max}}(h \rightarrow \chi_1^0 \chi_1^0) \sim \begin{cases} 0.8\% & m_\chi \approx 60 \text{ GeV}, \\ 8\% & m_\chi \approx 45 \text{ GeV}. \end{cases} \quad (5.3)$$

The branching fraction near 60 GeV is rather small although this is clearly identifiable as the h -funnel region. The branching fraction near 45 GeV is about an order of magnitude larger because of the available kinematics, even though it is from the Z -funnel. This leads to the very interesting and challenging possibility of observing the Higgs invisible decay at the LHC [101–103], (a sensitivity of about 20% is considered feasible). The search sensitivity would be significantly improved at future e^+e^- colliders, reaching about a few percent at the International Linear Collider (ILC), and even 0.3% at the TLEP [104].

Type labels	DM mass $m_{\chi_1^0}$	Annihilation channels	Partial waves	$\langle\sigma v\rangle(v \rightarrow 0)$	Collider searches
I-A	$\sim m_Z/2$	$\chi_1^0\chi_1^0 \rightarrow Z$	p	low	$h, H, A \rightarrow \chi_1^0\chi_1^0$
I-B	$\sim m_h/2$	$\chi_1^0\chi_1^0 \rightarrow h$	p	low	$H, A \rightarrow \chi_1^0\chi_1^0$
I-C	$\sim m_A/2$	$\chi_1^0\chi_1^0 \rightarrow A, H$	s, p	high	
II-A	$m_{\chi_1^0} \sim m_{\chi_1^\pm}$ $\sim m_{\chi_2^0}$	$\chi_1^0\chi_2^0, \chi_1^0\chi_1^\pm$ $\chi_2^0\chi_2^0, \chi_1^\pm\chi_1^\mp$ $\rightarrow SM$	s+p	medium	$H, A \rightarrow \chi_1^0\chi_2^0$ $H, A \rightarrow \chi_2^0\chi_2^0$ $H^\pm \rightarrow \chi_1^0\chi_1^\pm$
II-B	$m_{\chi_1^0} \sim m_{\tilde{\tau}_1}$ $\sim m_{\tilde{\nu}_\tau}$	$\tilde{\tau}_1^+\tilde{\tau}_1^-, \tilde{\nu}_\tau\tilde{\nu}_\tau,$ $\chi_1^0\tilde{\tau}_1^\pm \rightarrow SM$	s+p	medium	$H, A \rightarrow \tilde{\tau}_1^+\tilde{\tau}_1^-$ $H^\pm \rightarrow \tilde{\tau}_1^\pm\tilde{\nu}_\tau$

Table 1: Connection between the SUSY DM properties and Higgs bosons.

5.5 Consequences of co-annihilation

For the co-annihilation scenarios, the other lower-lying SUSY particles are nearly degenerate with the LSP to ensure efficient annihilation. The common case is that the NLSP and NNLSP of the Winos (χ_1^\pm, χ_2^0) or the Higgsinos ($\chi_1^\pm, \chi_{2,3}^0$) are nearly degenerate with the Bino-like LSP, with appreciable mixing among them. On the other hand, the XENON-100 search bound puts a constraint on the sizes of the mixing as seen from Fig 7(a) and (b). Nevertheless, the spin-independent cross sections are typically higher than those from the Higgs resonances, reaching $\sigma_p^{\text{SI}} \sim 10^{-8}$ pb (yellow region). The indirect detection cross sections are in general between the s -wave dominance (higher green band) and p -wave dominance (lower green band).

As shown in Figs. 9(b)–(d), branching fractions for the other heavy Higgs bosons H, A to a pair of light SUSY particles could reach up to about 10% – 20%. These are the solutions for the correct relic density with co-annihilations. However, due to the mass degeneracy, the final decay products would be rather soft and are difficult to observe with the LHC. Consequently, these also yield the invisible decay channels.

The coannihilation scenarios predict a rich spectrum near the LSP mass, leading to many different phenomena that can be explored by particles pair productions [66, 105].

6. Summary and Conclusions

Within the framework of the minimal supersymmetric extension of the standard model (MSSM), we investigated the possibility of the lightest supersymmetric particle being all the dark matter in light of the recent discovery of a SM-like Higgs boson, and the search for other Higgs bosons and SUSY particles at the LHC. We scanned through a wide range of the MSSM parameter space, and searched for model points wherein LSP has the correct properties to be the (WIMP) thermal DM. We studied the freeze-out of WIMPs and computed the cross section required to give the correct DM relic abundance in terms of velocity-independent and velocity-dependent components. We applied the constraints on the MSSM Higgs sector from the LEP, Tevatron and LHC observations. We also imposed

flavor constraints from the recent experimental results at the LHCb and BELLE, and found stringent bounds on the parameter space. The low LSP mass region is essentially closed, yielding a rough bound $m_\chi > 30$ GeV. We thus find that the DAMA/CoGeNT/CRESST observations are incompatible with the MSSM.

The XENON-100 experiment significantly constrains the viable parameter region via the spin-independent elastic WIMP-proton scattering cross section. We are able to identify the Higgs contributions and thus to make predictions for future searches at the LHC. There are also clear contributions from the co-annihilation channels. Table 1 summarizes these distinctive MSSM model points, and the relation with the Higgs bosons. We reiterate the key points of our findings. For the resonance scenarios as in I-A, I-B, and I-C,

- Z , h , H and A are the most important mediators at resonance to yield the correct relic abundance and give predictive narrow mass windows as shown in Fig. 5, which we refer to as the Z , h and H/A -funnel regions. It is interesting to note that the spin-independent scattering in the Z, h funnel can be dominated by the t -channel H exchange when $N_{13}^2 \gg N_{14}^2$.
- With our parameter scanning, the necessarily non-zero Wino, Higgsino components of the LSP imply a lower bound for the WIMP scattering cross section mediated by h and H , as in Eq. (5.2). In particular, the spin-independent cross sections may be fully covered by the next generation of direct search experiments for DM mass around 30 – 800 GeV such as LUX and XENON-1T. An exception is the fine-tuned cancellation, the “blind spots” scenario, way above the Z, h funnels.
- Z , h , H and A mediators determine the partial wave decomposition as listed in Table 1 and predict a definite range of indirect search cross sections. It is especially sensitive to the A -exchange contribution, seen in Fig. 8(a).
- The invisible decays of h , H , A and H^\pm are expected, and plotted in Fig. 9(a). Future searches at the LHC, and in particular, searches at the ILC may reveal the true nature of the DM particle.

For the co-annihilation scenarios as in II-A and II-B,

- Although the “well-tempered” scenario with large Higgsino and Wino fractions is disfavored by the XENON-100 data, the co-annihilation may still be a valid solution to obtain the correct relic density. There may be several light SUSY particles such as neutralinos, charginos, or stau, leading to many rich phenomena that can be explored at collider experiments.
- For highly degenerate NLSP, NNLSP, the decays of H , A and H^\pm as shown in Figs. 9(b)-(d) could lead to large invisible modes, making the collider search for DM very interesting.

We conclude that understanding the nature of DM requires us to consider results from a number of different experiments. Future collider searches and the next generation

of direct detection experiments will likely cover the conventional parameter range of the MSSM if the LSP constitutes all of the DM. The recent exciting discovery of the SM-like Higgs boson, and searches for beyond the SM physics at the energy frontier will serve as a new “lamp post” and guide in DM searches complementary to what may be obtained from direct detection and astro-particle observations at the cosmic frontier.

Acknowledgments

We would like to thank M. Drees, B. Dutta, G. Gelmini, J. Fan, L. Roszkowski, J. Ruderman, S. Su and X. Tata for helpful discussions. T.H. and Z.L. are supported in part by the U.S. Department of Energy under Grant No. DE-FG02-95ER40896, in part by the PITT PACC. Z.L. is also supported in part by the LHC Theory Initiative from the U.S. National Science Foundation under Grant No. NSF-PHY-0969510. A.N. is supported in part by a McWilliams postdoctoral fellowship awarded by the Bruce and Astrid McWilliams Center for Cosmology, and in part by NSF grant AST-1211777. T.H. would also like to thank the Aspen Center for Physics for the hospitality during which part of the work was carried out. The Aspen Center for Physics is supported by the NSF under Grant No.1066293.

References

- [1] G. Jungman, M. Kamionkowski, and K. Griest, *Supersymmetric dark matter*, *Phys.Rept.* **267** (1996) 195–373, [[hep-ph/9506380](#)].
- [2] G. Bertone, D. Hooper, and J. Silk, *Particle dark matter: Evidence, candidates and constraints*, *Phys.Rept.* **405** (2005) 279–390, [[hep-ph/0404175](#)].
- [3] M. Drees and G. Gerbier, *Mini-Review of Dark Matter: 2012*, [arXiv:1204.2373](#).
- [4] **DAMA, LIBRA Collaboration** Collaboration, R. Bernabei et al., *New results from DAMA/LIBRA*, *Eur.Phys.J.* **C67** (2010) 39–49, [[arXiv:1002.1028](#)].
- [5] **CoGeNT Collaboration**, C. Aalseth, P. Barbeau, J. Colaresi, J. Collar, J. Diaz Leon, et al., *Search for an Annual Modulation in a P-type Point Contact Germanium Dark Matter Detector*, *Phys.Rev.Lett.* **107** (2011) 141301, [[arXiv:1106.0650](#)].
- [6] **CRESST Collaboration**, G. Angloher et al., *Results from 730 kg days of the CRESST-II Dark Matter Search*, *Eur.Phys.J.* **C72** (2012) 1971, [[arXiv:1109.0702](#)].
- [7] **XENON10 Collaboration**, J. Angle et al., *A search for light dark matter in XENON10 data*, *Phys.Rev.Lett.* **107** (2011) 051301, [[arXiv:1104.3088](#)].
- [8] **XENON100 Collaboration**, E. Aprile et al., *Dark Matter Results from 225 Live Days of XENON100 Data*, *Phys.Rev.Lett.* **109** (2012) 181301, [[arXiv:1207.5988](#)].
- [9] **CDMS Collaboration**, Z. Ahmed et al., *Search for annual modulation in low-energy CDMS-II data*, [arXiv:1203.1309](#).
- [10] **LUX Collaboration**, D. Akerib et al., *The Large Underground Xenon (LUX) Experiment*, [arXiv:1211.3788](#).
- [11] **XENON1T Collaboration**, E. Aprile, *The XENON1T Dark Matter Search Experiment*, [arXiv:1206.6288](#).

- [12] **TEXONO Collaboration** Collaboration, H. Li et al., *Limits on spin-independent couplings of WIMP dark matter with a p-type point-contact germanium detector*, [arXiv:1303.0925](#).
- [13] **Fermi-LAT Collaboration**, M. Ackermann et al., *Constraining Dark Matter Models from a Combined Analysis of Milky Way Satellites with the Fermi Large Area Telescope*, *Phys.Rev.Lett.* **107** (2011) 241302, [[arXiv:1108.3546](#)].
- [14] **H.E.S.S. Collaboration**, A. Abramowski et al., *Search for photon line-like signatures from Dark Matter annihilations with H.E.S.S.*, *Phys.Rev.Lett.* **110** (2013) 041301, [[arXiv:1301.1173](#)].
- [15] **MAGIC Collaboration**, J. Aleksic et al., *Searches for Dark Matter annihilation signatures in the Segue 1 satellite galaxy with the MAGIC-I telescope*, *JCAP* **1106** (2011) 035, [[arXiv:1103.0477](#)].
- [16] **VERITAS Collaboration**, T. Arlen et al., *Constraints on Cosmic Rays, Magnetic Fields, and Dark Matter from Gamma-Ray Observations of the Coma Cluster of Galaxies with VERITAS and Fermi*, *Astrophys.J.* **757** (2012) 123, [[arXiv:1208.0676](#)].
- [17] **WMAP Collaboration**, D. Larson, J. Dunkley, G. Hinshaw, E. Komatsu, M. Nolte, et al., *Seven-Year Wilkinson Microwave Anisotropy Probe (WMAP) Observations: Power Spectra and WMAP-Derived Parameters*, *Astrophys.J.Suppl.* **192** (2011) 16, [[arXiv:1001.4635](#)].
- [18] G. Hinshaw, D. Larson, E. Komatsu, D. Spergel, C. Bennett, et al., *Nine-Year Wilkinson Microwave Anisotropy Probe (WMAP) Observations: Cosmological Parameter Results*, [arXiv:1212.5226](#).
- [19] S. Galli, F. Iocco, G. Bertone, and A. Melchiorri, *CMB constraints on Dark Matter models with large annihilation cross-section*, *Phys.Rev.* **D80** (2009) 023505, [[arXiv:0905.0003](#)].
- [20] G. Hutsi, J. Chluba, A. Hektor, and M. Raidal, *WMAP7 and future CMB constraints on annihilating dark matter: implications on GeV-scale WIMPs*, *Astron.Astrophys.* **535** (2011) A26, [[arXiv:1103.2766](#)].
- [21] S. Galli, F. Iocco, G. Bertone, and A. Melchiorri, *Updated CMB constraints on Dark Matter annihilation cross-sections*, *Phys.Rev.* **D84** (2011) 027302, [[arXiv:1106.1528](#)].
- [22] A. Natarajan, *A closer look at CMB constraints on WIMP dark matter*, *Phys.Rev.* **D85** (2012) 083517, [[arXiv:1201.3939](#)].
- [23] G. Giesen, J. Lesgourgues, B. Audren, and Y. Ali-Haïmoud, *CMB photons shedding light on dark matter*, *JCAP* **1212** (2012) 008, [[arXiv:1209.0247](#)].
- [24] C. Evoli, S. Pandolfi, and A. Ferrara, *CMB constraints on light dark matter candidates*, [arXiv:1210.6845](#).
- [25] A. Geringer-Sameth and S. M. Koushiappas, *Exclusion of canonical WIMPs by the joint analysis of Milky Way dwarfs with Fermi*, *Phys.Rev.Lett.* **107** (2011) 241303, [[arXiv:1108.2914](#)].
- [26] R. Cotta, A. Drlica-Wagner, S. Murgia, E. Bloom, J. Hewett, et al., *Constraints on the pMSSM from LAT Observations of Dwarf Spheroidal Galaxies*, *JCAP* **1204** (2012) 016, [[arXiv:1111.2604](#)].
- [27] J. L. Feng, K. T. Matchev, and F. Wilczek, *Neutralino dark matter in focus point supersymmetry*, *Phys.Lett.* **B482** (2000) 388–399, [[hep-ph/0004043](#)].

- [28] J. D. Wells, *PeV-scale supersymmetry*, *Phys.Rev.* **D71** (2005) 015013, [[hep-ph/0411041](#)].
- [29] N. Arkani-Hamed and S. Dimopoulos, *Supersymmetric unification without low energy supersymmetry and signatures for fine-tuning at the LHC*, *JHEP* **0506** (2005) 073, [[hep-th/0405159](#)].
- [30] G. Giudice and A. Romanino, *Split supersymmetry*, *Nucl.Phys.* **B699** (2004) 65–89, [[hep-ph/0406088](#)].
- [31] G. F. Giudice, T. Han, K. Wang, and L.-T. Wang, *Nearly Degenerate Gauginos and Dark Matter at the LHC*, *Phys.Rev.* **D81** (2010) 115011, [[arXiv:1004.4902](#)].
- [32] J. Ellis and K. A. Olive, *Revisiting the Higgs Mass and Dark Matter in the CMSSM*, *Eur.Phys.J.* **C72** (2012) 2005, [[arXiv:1202.3262](#)].
- [33] H. Baer, V. Barger, and A. Mustafayev, *Neutralino dark matter in mSUGRA/CMSSM with a 125 GeV light Higgs scalar*, *JHEP* **1205** (2012) 091, [[arXiv:1202.4038](#)].
- [34] A. Fowlie, A. Kalinowski, M. Kazana, L. Roszkowski, and Y. S. Tsai, *Bayesian Implications of Current LHC and XENON100 Search Limits for the Constrained MSSM*, *Phys.Rev.* **D85** (2012) 075012, [[arXiv:1111.6098](#)].
- [35] L. Roszkowski, E. M. Sessolo, and Y.-L. S. Tsai, *Bayesian Implications of Current LHC Supersymmetry and Dark Matter Detection Searches for the Constrained MSSM*, *Phys.Rev.* **D86** (2012) 095005, [[arXiv:1202.1503](#)].
- [36] H. Baer, V. Barger, P. Huang, and X. Tata, *Natural Supersymmetry: LHC, dark matter and ILC searches*, *JHEP* **1205** (2012) 109, [[arXiv:1203.5539](#)].
- [37] G. Belanger, S. Biswas, C. Boehm, and B. Mukhopadhyaya, *Light Neutralino Dark Matter in the MSSM and Its Implication for LHC Searches for Staus*, *JHEP* **1212** (2012) 076, [[arXiv:1206.5404](#)].
- [38] A. Arbey, M. Battaglia, A. Djouadi, and F. Mahmoudi, *The Higgs sector of the phenomenological MSSM in the light of the Higgs boson discovery*, *JHEP* **1209** (2012) 107, [[arXiv:1207.1348](#)].
- [39] H. Baer, V. Barger, A. Lessa, and X. Tata, *Discovery potential for SUSY at a high luminosity upgrade of LHC14*, *Phys.Rev.* **D86** (2012) 117701, [[arXiv:1207.4846](#)].
- [40] R. Allahverdi, B. Dutta, and K. Sinha, *Non-thermal Higgsino Dark Matter: Cosmological Motivations and Implications for a 125 GeV Higgs*, *Phys.Rev.* **D86** (2012) 095016, [[arXiv:1208.0115](#)].
- [41] S. Mohanty, S. Rao, and D. Roy, *Predictions of a Natural SUSY Dark Matter Model for Direct and Indirect Detection Experiments*, *JHEP* **1211** (2012) 175, [[arXiv:1208.0894](#)].
- [42] H. Baer, *Radiative natural supersymmetry with mixed axion/higgsino cold dark matter*, [arXiv:1210.7852](#).
- [43] J. Hisano, K. Ishiwata, and N. Nagata, *Direct Search of Dark Matter in High-Scale Supersymmetry*, [arXiv:1210.5985](#).
- [44] L. J. Hall, Y. Nomura, and S. Shirai, *Spread Supersymmetry with Wino LSP: Gluino and Dark Matter Signals*, [arXiv:1210.2395](#).
- [45] W. Altmannshofer, M. Carena, N. R. Shah, and F. Yu, *Indirect Probes of the MSSM after the Higgs Discovery*, *JHEP* **1301** (2013) 160, [[arXiv:1211.1976](#)].

- [46] M. W. Cahill-Rowley, J. L. Hewett, A. Ismail, and T. G. Rizzo, *More Energy, More Searches, but the p MSSM Lives On*, [arXiv:1211.1981](#).
- [47] A. Arbey, M. Battaglia, A. Djouadi, and F. Mahmoudi, *An update on the constraints on the phenomenological MSSM from the new LHC Higgs results*, *Physics Letters B* **720** (2013) , pp. 153–160, [[arXiv:1211.4004](#)].
- [48] C. Cheung, L. J. Hall, D. Pinner, and J. T. Ruderman, *Prospects and Blind Spots for Neutralino Dark Matter*, [arXiv:1211.4873](#).
- [49] C. Stenge, G. Bertone, F. Feroz, M. Fornasa, R. R. de Austri, et al., *Global Fits of the c MSSM and NUHM including the LHC Higgs discovery and new XENON100 constraints*, [arXiv:1212.2636](#).
- [50] Y.-L. S. Tsai, Q. Yuan, and X. Huang, *A generic method to constrain the dark matter model parameters from Fermi observations of dwarf spheroids*, [arXiv:1212.3990](#).
- [51] K. Kowalska, L. Roszkowski, and E. M. Sessolo, *Two ultimate tests of constrained supersymmetry*, [arXiv:1302.5956](#).
- [52] **Belle** Collaboration, P. Koppenburg et al., *An Inclusive measurement of the photon energy spectrum in $b \rightarrow s$ gamma decays*, *Phys.Rev.Lett.* **93** (2004) 061803, [[hep-ex/0403004](#)].
- [53] **LHCb** Collaboration, R. Aaij et al., *First evidence for the decay $B_s \rightarrow \mu^+ \mu^-$* , *Phys. Rev. Lett.* **110**, **021801** (2013) [[arXiv:1211.2674](#)].
- [54] M. Laine and Y. Schroder, *Quark mass thresholds in QCD thermodynamics*, *Phys.Rev.* **D73** (2006) 085009, [[hep-ph/0603048](#)].
- [55] J. R. Ellis, J. Hagelin, D. V. Nanopoulos, K. A. Olive, and M. Srednicki, *Supersymmetric Relics from the Big Bang*, *Nucl.Phys.* **B238** (1984) 453–476.
- [56] M. W. Goodman and E. Witten, *Detectability of Certain Dark Matter Candidates*, *Phys.Rev.* **D31** (1985) 3059.
- [57] K. Griest, *Cross-Sections, Relic Abundance and Detection Rates for Neutralino Dark Matter*, *Phys.Rev.* **D38** (1988) 2357.
- [58] R. Barbieri and G. Giudice, *Upper Bounds on Supersymmetric Particle Masses*, *Nucl.Phys.* **B306** (1988) 63.
- [59] R. Kitano and Y. Nomura, *Supersymmetry, naturalness, and signatures at the LHC*, *Phys.Rev.* **D73** (2006) 095004, [[hep-ph/0602096](#)].
- [60] V. Barger, P. Langacker, H.-S. Lee, and G. Shaughnessy, *Higgs Sector in Extensions of the MSSM*, *Phys.Rev.* **D73** (2006) 115010, [[hep-ph/0603247](#)].
- [61] M. W. Cahill-Rowley, J. L. Hewett, A. Ismail, and T. G. Rizzo, *The Higgs Sector and Fine-Tuning in the p MSSM*, *Phys.Rev.* **D86** (2012) 075015, [[arXiv:1206.5800](#)].
- [62] J. L. Feng, *Naturalness and the Status of Supersymmetry*, [arXiv:1302.6587](#).
- [63] N. Arkani-Hamed, A. Delgado, and G. Giudice, *The Well-tempered neutralino*, *Nucl.Phys.* **B741** (2006) 108–130, [[hep-ph/0601041](#)].
- [64] M. Perelstein and B. Shakya, *Fine-Tuning Implications of Direct Dark Matter Searches in the MSSM*, *JHEP* **1110** (2011) 142, [[arXiv:1107.5048](#)].

- [65] **CMS Collaboration** Collaboration, S. Chatrchyan et al., *Search for electroweak production of charginos and neutralinos using leptonic final states in pp collisions at $\sqrt{s} = 7$ TeV*, *JHEP* **1211** (2012) 147, [[arXiv:1209.6620](#)].
- [66] T. Han, S. Padhi, and S. Su, *Charginos and Neutralinos in the Light of the Higgs Boson, work in progress*, .
- [67] A. Chatterjee, M. Drees, and S. Kulkarni, *Radiative Corrections to the Neutralino Dark Matter Relic Density - an Effective Coupling Approach*, *Phys.Rev.* **D86** (2012) 105025, [[arXiv:1209.2328](#)].
- [68] S. Heinemeyer, W. Hollik, and G. Weiglein, *FeynHiggs: A Program for the calculation of the masses of the neutral CP even Higgs bosons in the MSSM*, *Comput.Phys.Commun.* **124** (2000) 76–89, [[hep-ph/9812320](#)].
- [69] P. Bechtle, O. Brein, S. Heinemeyer, G. Weiglein, and K. E. Williams, *HiggsBounds: Confronting Arbitrary Higgs Sectors with Exclusion Bounds from LEP and the Tevatron*, *Comput.Phys.Commun.* **181** (2010) 138–167, [[arXiv:0811.4169](#)].
- [70] B. Allanach, C. Balazs, G. Belanger, M. Bernhardt, F. Boudjema, et al., *SUSY Les Houches Accord 2*, *Comput.Phys.Commun.* **180** (2009) 8–25, [[arXiv:0801.0045](#)].
- [71] G. Belanger, F. Boudjema, A. Pukhov, and A. Semenov, *MicrOMEGAs 2.0: A Program to calculate the relic density of dark matter in a generic model*, *Comput.Phys.Commun.* **176** (2007) 367–382, [[hep-ph/0607059](#)].
- [72] R. Barbieri and G. Giudice, *$b \rightarrow s$ gamma decay and supersymmetry*, *Phys.Lett.* **B309** (1993) 86–90, [[hep-ph/9303270](#)].
- [73] **Heavy Flavor Averaging Group** Collaboration, Y. Amhis et al., *Averages of B-Hadron, C-Hadron, and tau-lepton properties as of early 2012*, [arXiv:1207.1158](#).
- [74] M. Misiak, H. Asatrian, K. Bieri, M. Czakon, A. Czarnecki, et al., *Estimate of $B(\text{anti-}B \rightarrow X(s) \text{ gamma})$ at $O(\alpha(s)^{**2})$* , *Phys.Rev.Lett.* **98** (2007) 022002, [[hep-ph/0609232](#)].
- [75] T. Becher and M. Neubert, *Analysis of $Br(\text{anti-}B \rightarrow X(s) \text{ gamma})$ at NNLO with a cut on photon energy*, *Phys.Rev.Lett.* **98** (2007) 022003, [[hep-ph/0610067](#)].
- [76] M. Benzke, S. J. Lee, M. Neubert, and G. Paz, *Factorization at Subleading Power and Irreducible Uncertainties in $\bar{B} \rightarrow X_s \gamma$ Decay*, *JHEP* **1008** (2010) 099, [[arXiv:1003.5012](#)].
- [77] K. Babu and C. F. Kolda, *Higgs mediated $B^0 \rightarrow \mu^+ \mu^-$ in minimal supersymmetry*, *Phys.Rev.Lett.* **84** (2000) 228–231, [[hep-ph/9909476](#)].
- [78] A. J. Buras, J. Gierbach, D. Guadagnoli, and G. Isidori, *On the Standard Model prediction for $BR(Bs, d \text{ to } \mu^+ \mu^-)$* , *Eur.Phys.J.* **C72** (2012) 2172, [[arXiv:1208.0934](#)].
- [79] **Super-Kamiokande** Collaboration, S. Desai et al., *Search for dark matter WIMPs using upward through-going muons in Super-Kamiokande*, *Phys.Rev.* **D70** (2004) 083523, [[hep-ex/0404025](#)].
- [80] **IceCube** Collaboration, M. Aartsen et al., *Search for dark matter annihilations in the Sun with the 79-string IceCube detector*, [arXiv:1212.4097](#).
- [81] N. D. Christensen, T. Han, and S. Su, *MSSM Higgs Bosons at The LHC*, *Phys.Rev.* **D85** (2012) 115018, [[arXiv:1203.3207](#)].

- [82] M. Carena, S. Heinemeyer, O. Staal, C. Wagner, and G. Weiglein, *MSSM Higgs Boson Searches at the LHC: Benchmark Scenarios after the Discovery of a Higgs-like Particle*, [arXiv:1302.7033](#).
- [83] T. Han, T. Li, L. Wang, and S. Su, *SUSY Implications for Non-Decoupling Higgs Sector*, *work in progress*, .
- [84] J. R. Ellis, K. A. Olive, and C. Savage, *Hadronic Uncertainties in the Elastic Scattering of Supersymmetric Dark Matter*, *Phys.Rev.* **D77** (2008) 065026, [[arXiv:0801.3656](#)].
- [85] E. Accomando, R. L. Arnowitt, B. Dutta, and Y. Santoso, *Neutralino proton cross-sections in supergravity models*, *Nucl.Phys.* **B585** (2000) 124–142, [[hep-ph/0001019](#)].
- [86] J. Edsjo and P. Gondolo, *Neutralino relic density including coannihilations*, *Phys.Rev.* **D56** (1997) 1879–1894, [[hep-ph/9704361](#)].
- [87] J. Edsjo, M. Schelke, P. Ullio, and P. Gondolo, *Accurate relic densities with neutralino, chargino and sfermion coannihilations in mSUGRA*, *JCAP* **0304** (2003) 001, [[hep-ph/0301106](#)].
- [88] J. R. Ellis, T. Falk, and K. A. Olive, *Neutralino - Stau coannihilation and the cosmological upper limit on the mass of the lightest supersymmetric particle*, *Phys.Lett.* **B444** (1998) 367–372, [[hep-ph/9810360](#)].
- [89] J. R. Ellis, T. Falk, K. A. Olive, and M. Srednicki, *Calculations of neutralino-stau coannihilation channels and the cosmologically relevant region of MSSM parameter space*, *Astropart.Phys.* **13** (2000) 181–213, [[hep-ph/9905481](#)].
- [90] J. R. Ellis, K. A. Olive, and Y. Santoso, *Calculations of neutralino stop coannihilation in the CMSSM*, *Astropart.Phys.* **18** (2003) 395–432, [[hep-ph/0112113](#)].
- [91] M. Srednicki and R. Watkins, *Coherent Couplings Of Neutralinos To Nuclei From Squark Mixing*, *Phys.Lett.* **B225** (1989) 140.
- [92] G. Gelmini, P. Gondolo, and E. Roulet, *Neutralino dark matter searches*, *Nucl.Phys.* **B351** (1991) 623–644.
- [93] M. Drees and M. M. Nojiri, *Neutralino relic density in minimal $n = 1$ supergravity*, *Phys. Rev. D* **47** (Jan, 1993) 376–408.
- [94] M. Drees and M. M. Nojiri, *New contributions to coherent neutralino - nucleus scattering*, *Phys.Rev.* **D47** (1993) 4226–4232, [[hep-ph/9210272](#)].
- [95] M. Drees and M. Nojiri, *Neutralino - nucleon scattering revisited*, *Phys.Rev.* **D48** (1993) 3483–3501, [[hep-ph/9307208](#)].
- [96] J. R. Ellis, A. Ferstl, and K. A. Olive, *Reevaluation of the elastic scattering of supersymmetric dark matter*, *Phys.Lett.* **B481** (2000) 304–314, [[hep-ph/0001005](#)].
- [97] *Search for direct top squark pair production in events with a single isolated lepton, jets and missing transverse energy at $\sqrt{s} = 8$ tev*, Tech. Rep. CMS-PAS-SUS-12-023, CERN, Geneva, 2012.
- [98] **ATLAS** Collaboration, G. Aad et al., *Multi-channel search for squarks and gluinos in $\sqrt{s} = 7$ TeV pp collisions with the ATLAS detector*, [arXiv:1212.6149](#).
- [99] Y. G. Kim, T. Nihei, L. Roszkowski, and R. Ruiz de Austri, *Upper and lower limits on neutralino WIMP mass and spin independent scattering cross-section, and impact of new $(g-2)(\mu)$ measurement*, *JHEP* **0212** (2002) 034, [[hep-ph/0208069](#)].

- [100] V. Barger, W.-Y. Keung, and G. Shaughnessy, *Spin Dependence of Dark Matter Scattering*, *Phys.Rev.* **D78** (2008) 056007, [[arXiv:0806.1962](#)].
- [101] H. Davoudiasl, T. Han, and H. E. Logan, *Discovering an invisibly decaying Higgs at hadron colliders*, *Phys.Rev.* **D71** (2005) 115007, [[hep-ph/0412269](#)].
- [102] Y. Bai, P. Draper, and J. Shelton, *Measuring the Invisible Higgs Width at the 7 and 8 TeV LHC*, *JHEP* **1207** (2012) 192, [[arXiv:1112.4496](#)].
- [103] G. Belanger, B. Dumont, U. Ellwanger, J. Gunion, and S. Kraml, *Status of invisible Higgs decays*, [arXiv:1302.5694](#).
- [104] A. Blondel, A. Chao, W. Chou, J. Gao, D. Schulte, et al., *Report of the ICFA Beam Dynamics Workshop 'Accelerators for a Higgs Factory: Linear vs. Circular' (HF2012)*, [arXiv:1302.3318](#).
- [105] B. Dutta, T. Kamon, N. Koley, K. Sinha, K. Wang, et al., *Top Squark Searches Using Dilepton Invariant Mass Distributions and Bino-Higgsino Dark Matter at the LHC*, [arXiv:1302.3231](#).
- [106] G. Steigman, B. Dasgupta, and J. F. Beacom, *Precise Relic WIMP Abundance and its Impact on Searches for Dark Matter Annihilation*, *Phys.Rev.* **D86** (2012) 023506, [[arXiv:1204.3622](#)].

Appendix

A. Relic density calculation

When the Hubble expansion $H = \dot{a}/a$ became much larger than the interaction rate $\Gamma = n_\chi \langle \sigma_a v \rangle$, the WIMPs (χ^0), once in thermal equilibrium with the rest of the Universe, decoupled from equilibrium. The number density of WIMPs at a time t , $n_\chi(t)$, is obtained by solving the Boltzmann equation

$$\frac{1}{a^3} \frac{d(a^3 n_\chi)}{dt} = -\langle \sigma_a v \rangle [n_\chi^2 - n_{\text{eq}}^2], \quad (\text{A.1})$$

where $\langle \sigma_a v \rangle$ is the WIMP annihilation rate averaged over velocities, and n_{eq} is the equilibrium number density of WIMPs:

$$n_{\text{eq}} = \frac{g}{2\pi^2} \int_{m_\chi}^{\infty} dE \frac{E \sqrt{E^2 - m_\chi^2}}{1 + e^{E/T}}. \quad (\text{A.2})$$

g measures the number of relativistic degrees of freedom, and T is the temperature.

Define the dimensionless variables $Y = n_\chi/s$ and $x = m_\chi/T$, where s is the entropy density given by

$$s = \frac{2\pi^2}{45} g_s T^3. \quad (\text{A.3})$$

Here and henceforth, we adopt the natural units $k_b = \hbar = c = 1$. g_s is different from g only at late times, after neutrinos have decoupled from equilibrium, and e^\pm annihilation leads to the photons being heated relative to the neutrinos. However, dY/dx is very small at late

times, and with good accuracy, we may set $g = g_s$ when computing the relic abundance. The entropy per comoving volume is conserved, and hence

$$\frac{d(a^3 s)}{dt} = \frac{d(g a^3 T^3)}{dt} = 0 \quad (\text{A.4})$$

We may then rewrite Eq. (A.1) in terms of Y as:

$$\frac{dY}{dt} = -\langle \sigma_a v \rangle s [Y^2 - Y_{\text{eq}}^2], \quad (\text{A.5})$$

where $Y_{\text{eq}} = n_{\text{eq}}/s$. From Eq. (A.4), we see that $g a^3 T^3 = \text{constant}$, and therefore,

$$-\frac{\dot{T}}{T} = H + \frac{\dot{g}}{3g}. \quad (\text{A.6})$$

The Hubble parameter $H(T)$ is given by the expression

$$H = \left[\frac{8\pi G}{3} \rho_\gamma \right]^{1/2} = \left[\frac{8\pi^3 G}{90} \right]^{1/2} g^{1/2} T^2 \quad (\text{A.7})$$

Differentiating $x = m_\chi/T$ with respect to time, we find

$$\begin{aligned} \dot{x} &= \left(-\dot{T}/T \right) x = Hx \left[1 + \frac{\dot{g}_s}{3Hg_s} \right] \\ &\approx Hx \left[1 - \frac{1}{3} \frac{d(\ln g_s)}{d(\ln T)} \right], \end{aligned} \quad (\text{A.8})$$

where we simplified the second term on line 1 by substituting $\dot{x} \approx Hx$ (provided $\dot{g}_s \ll 3Hg_s$), and therefore $\dot{g} \approx -HT(dg/dT)$ [106]. Note that g changes significantly at the epoch of quark-hadron transition. We may now rewrite Eq. (A.5) in terms of x :

$$\begin{aligned} \frac{dY}{dx} &= \frac{-\langle \sigma_a v \rangle s(x)}{H(x)x \left[1 - \frac{1}{3} \frac{d(\ln g)}{d(\ln T)} \right]} \\ &= -\sqrt{\frac{\pi}{45G}} \langle \sigma_a v \rangle m_\chi \frac{g^{1/2}}{\left[1 - \frac{1}{3} \frac{d(\ln g)}{d(\ln T)} \right]} \frac{Y^2 - Y_{\text{eq}}^2}{x^2}. \end{aligned} \quad (\text{A.9})$$

We solve Eq. (A.9) numerically to obtain the present day value Y_0 , once the form of $g(T)$ and $\langle \sigma_a v \rangle$ are known. The dark matter relic density is then computed as:

$$\Omega_\chi h^2 = \frac{m_\chi Y_0 s_0}{(\rho_{\text{crit}}/h^2)}, \quad (\text{A.10})$$

where $s_0 \approx 2893 \text{ cm}^{-3}$ is the present day entropy density and $\rho_{\text{crit}} \approx 1.054 \times 10^{-5} h^2 \text{ GeV/cm}^3$ is the critical density.

After performing a numerical integration of the Boltzmann equation as formulated in Eq. (A.9), we show the WIMP number density in Fig. 10(a) and the WIMP relic (mass) density in Fig. 10(b), for various WIMP mass values. The dark straight-falling line gives

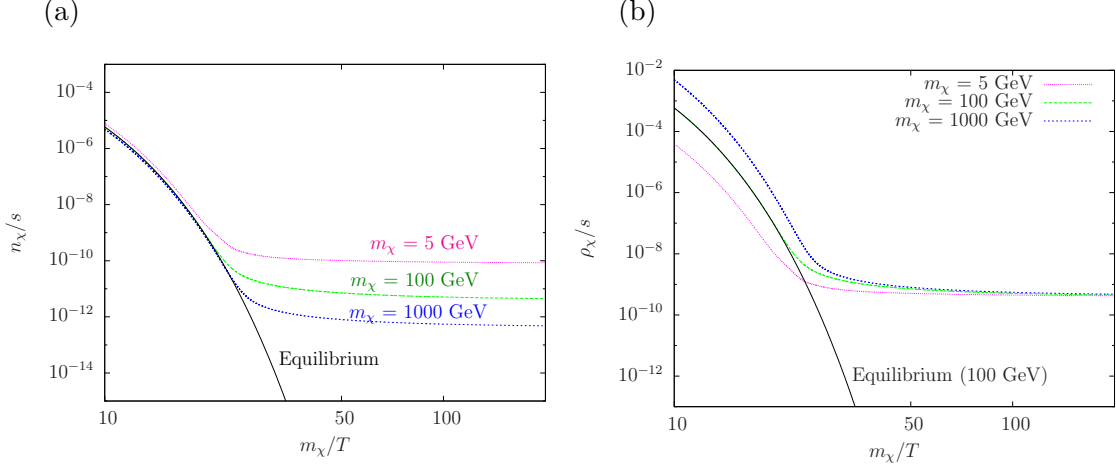


Figure 10: Evolution with temperature and yielding the correct WIMP relic density $\Omega_\chi h^2 = 0.11$ with illustrative values of the WIMP mass $m_\chi = 5, 100, \text{ and } 1000$ GeV, (a) WIMP number density, and (b) WIMP mass density. The equilibrium lines are for $m_\chi = 100$ GeV.

the densities if the particle keeps in thermal equilibrium with the environment for $m_\chi = 100$ GeV. It is known that the freeze-out temperature for a relatively light WIMP particle is

$$x_f = m_\chi/T \approx 20. \quad (\text{A.11})$$

The horizontal curves in Figs. 10(a) and (b) present the WIMP number density and mass density after freeze-out for $m_\chi = 5 - 1000$ GeV, leading to the correct relic density.